EAGE

Th CO2 P04

Numerical Analysis Of Immiscible/Near-Miscible CO2-WAG Displacement, Incorporating Compositional And Interfacial Tension Effects

G. Wang[1]*, G. Pickup[1], K. Sorbie[1], E. Mackay[1]
[1]Heriot-Watt University

Summary

The central objective of this paper is to study the balance and interactions of the different mechanistic contributions to the physics occurring during oil displacement by CO2 (both continuous and WAG). Mechanism 1 (M1) is the conventional oil stripping/compositional effect and Mechanism 2 (M2) is the near-miscible IFT effect on oil relative permeability through enhanced layer flow. Using sufficiently fine-scale models, we explain how these mechanisms interact with each other and affect the sweep and local displacement efficiency in a heterogeneous permeability field. We believe that studying the key processes separately leads to a greater insight into the physics of CO2 displacement, and this will help us to simulate the transition from immiscible to miscible displacement consistently at larger scales.

Introduction

During the transition from immiscible to miscible CO_2 WAG displacement, there are two mechanisms occurring, which are particularly important regarding the improvement of displacement performance, namely compositional effects (oil stripping, M1) and low interfacial tension effects (IFT effects, M2) (Sorbie and van Dijke 2010, Sohrabi et al. 2008a, Orr 2007). As CO_2 contacts in-situ oil, light-medium oil components are vaporised and produced with CO_2 (M1) as "gas" (supercritical fluid in fact), similar to chromatography (Orr 2007). At the same time, interfacial tension between gas and oil (σ_{go}) is also greatly changed due to the process of component transfer. As a result, the relative permeability gradually becomes linear (M2) when interfacial tension is close to zero under certain conditions (Stalkup 1983). Here, we simulated possible scenarios that are under the control of either/both mechanisms and investigated the flow behaviour and its effects on the distribution of the residual oil and ultimate oil recovery. Our aim is to develop a workflow incorporating these two mechanisms to improve simulations of near-miscible displacement (Figure 1).

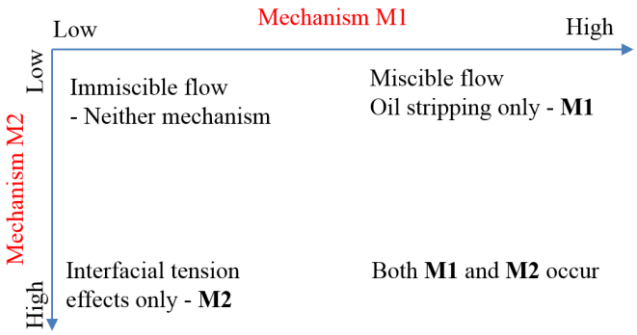

Figure 1 *Schematic of the research map.*

Methodology

A heterogeneous permeability field was generated with a Dykstra-Parsons (VDP) coefficient of 0.7 (Dykstra and Parsons 1950) and dimensionless correlation range (RL) of 0.1 (Figure 2). This model has a relatively short correlation length (1/10 of system length), and was generated to trigger possible fingering flow. Both wells were horizontal and were perforated along the width of the model. The injector in our tests was set to inject displacing fluid at a rate of 0.4 PV/d. and the producer was controlled by setting the minimum bottom-hole pressure. Two pore volumes injected (PVI) were simulated with the injection strategy as in Table 1 at both immiscible (70 bar) and near-miscible conditions (120 bar). This injection strategy was designed to allow us to analyse the flow behaviours of interest, such as fingering flow, improvement of sweep by WAG and the ultimate distribution of residual oil (Table 1).

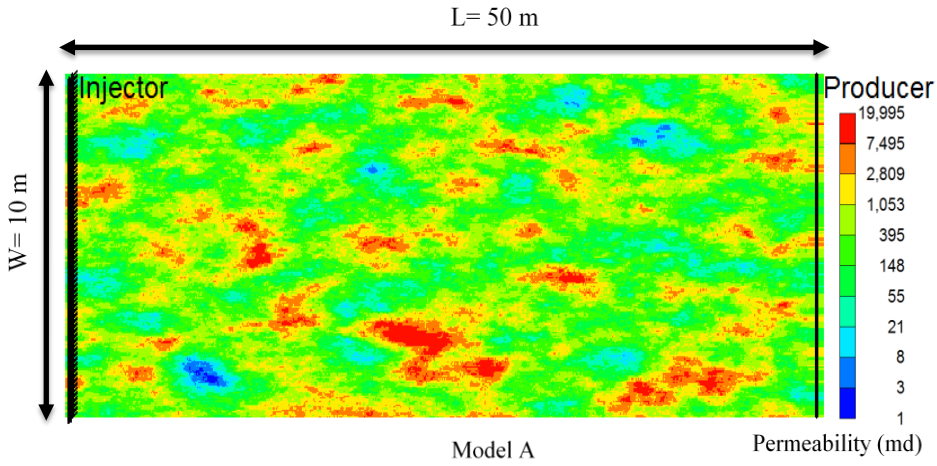

Figure 2 *Permeability Field A (VDP=0.7, RL=0.1) used to trigger fingering flow.*

WAG injection (2 PVI in total)	1st water cycle	1st gas cycle	2nd water cycle	2nd gas cycle	3rd water cycle
	0.4 PVI water	0.4 PVI CO_2	0.4 PVI water	0.4 PVI CO_2	0.4 PVI water

Table 1 *Injection strategy.*

The modelling of interfacial tension effects was carried out with the method implemented in CMG/GEM, which is based on Coats' model (Coats 1980). This method entails an interpolation between immiscible (Figure 3) and miscible relative permeabilities, with the use of a weighting function (CMG 2017). Three-phase relative permeabilities were calculated with one of the most widely-applied methods, Stone 2 (Aziz and Settari 1979). A typical light oil with a bubble point pressure of 38.5 bar at 53 °C and a viscosity of 0.16 mPa·s was used in our study. Here, compositional effects were modelled using the Peng-Robinson equation of state. The minimum miscibility pressure (MMP) is ~120 bar for this light oil. The complete dataset of this study, including the full fluid data, can be found online through the DOI: 10.17861/fc1c90bb-9d3f-4a6c-9170-7b7fe10ec7b9.

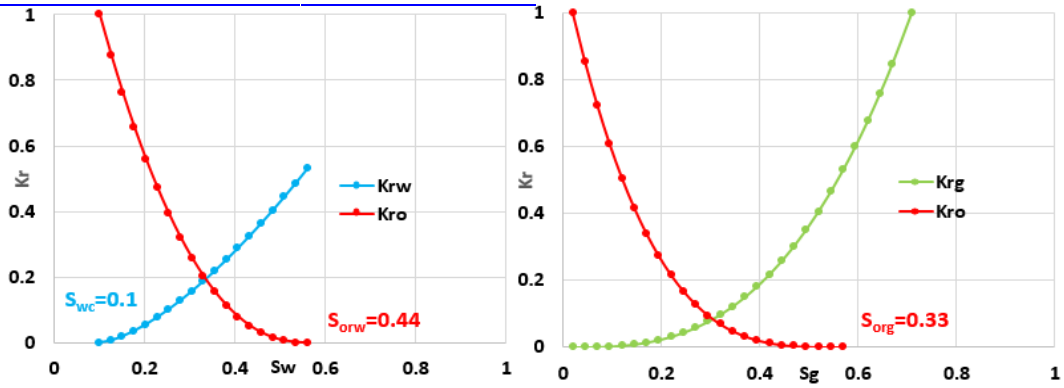

Figure 3 *Oil-water and oil-gas relative permeability curves.*

We set our base case as the immiscible WAG displacement (weak oil-stripping effects) without taking into account IFT effects. Then strong oil stripping effects and IFT effects were superimposed on the base case, respectively, through increasing the system pressure and varying the relative permeability with IFT, using the method implemented in GEM/CMG.

Results and discussions

Comparison of stability of gas displacing front

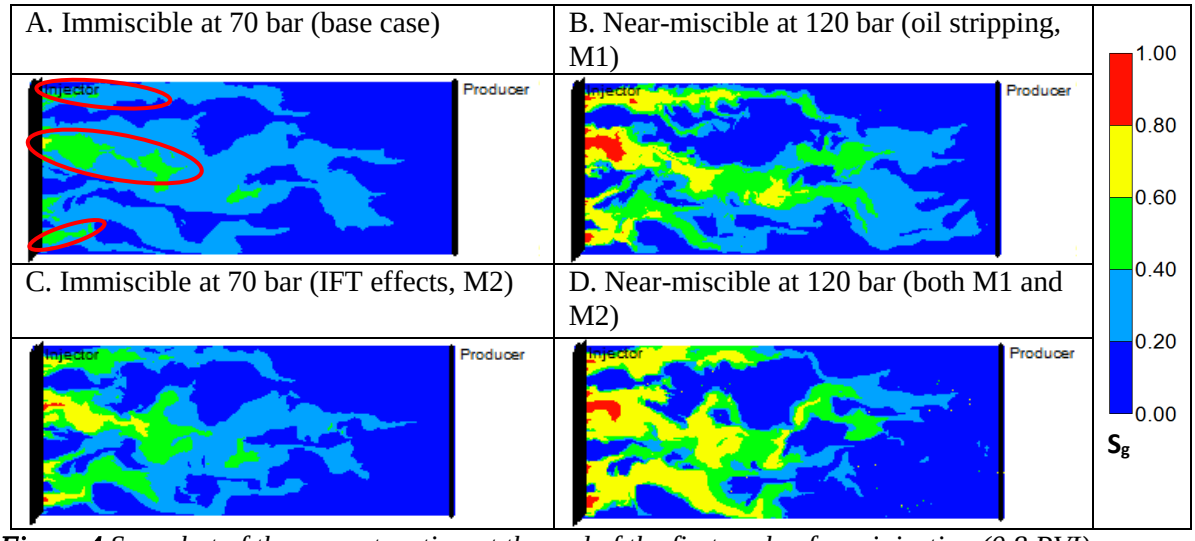

Figure 4 *Snapshot of the gas saturation at the end of the first cycle of gas injection (0.8 PVI).*

As expected, fingering flow occurs in all cases due to the unfavourable mobility ratio. Multiple preferential routes can be seen as indicated by the oval shapes. Very importantly, the viscous instability is observed to be more severe near the injector when taking one of the mechanisms into account (Figure 4 B and C). With oil stripping effects (Figure 4B), light-medium oil components are vaporized leading to higher gas saturation. With IFT effects (M2), more oil is mobilized and recovered allowing more gas to flow into these regions (Figure 4C). The consequent higher gas saturation (S_g) from both mechanisms leads to more severe gas fingers and therefore aggravates the imbalance of the fluid flow between preferential routes and non-preferential routes. Eventually, the combined mechanisms result in an even larger yellow area (Sg=0.6-0.8) in the preferential routes than the rest of cases (Figure 4D).

Comparison of displacement performance at the end (2 PVI).

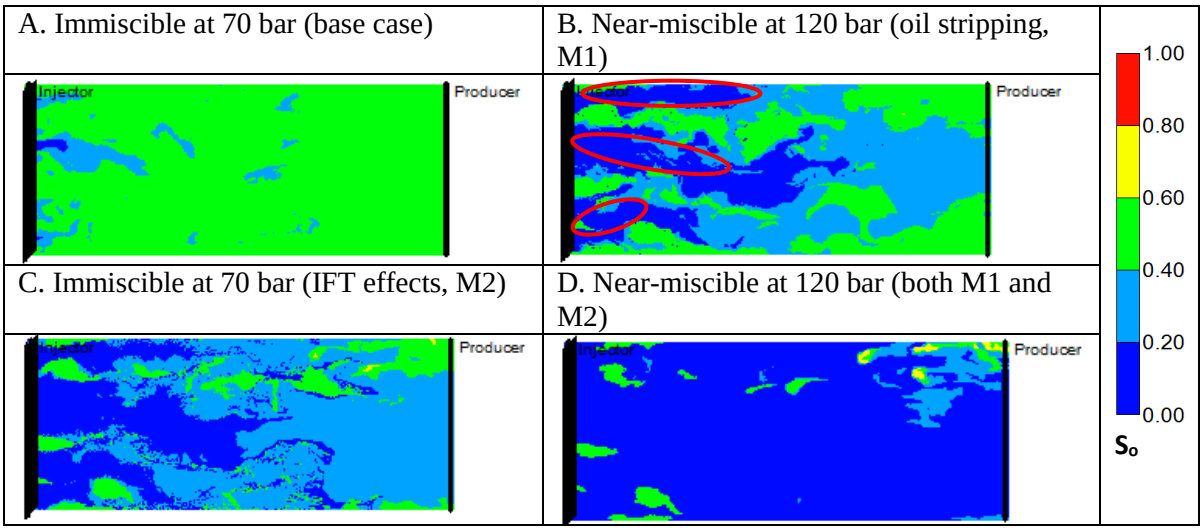

Figure 5 *Snapshot of the oil saturation at the end of injection (2 PVI).*

As seen in Figure 5A, the base case still has a large amount of remaining oil. The minor stripping effects are only able to achieve a very small region of low remaining oil saturation (S_o<0.2) near the injector. The whole system is mainly under the control of initial relative permeability with S_{org} of 0.33 and S_{orw} of 0.44. When the system pressure is increased to 120 bar (Figure 5B), oil stripping effects (M1) greatly improve the displacement efficiency in the preferential routes (oval shapes) but have limited impacts in the non-preferential routes. Since the process of oil stripping is highly dependent on the continuous contact between oil and CO_2, the local displacement performance is fairly poor in the non-preferential routes of gas flow.

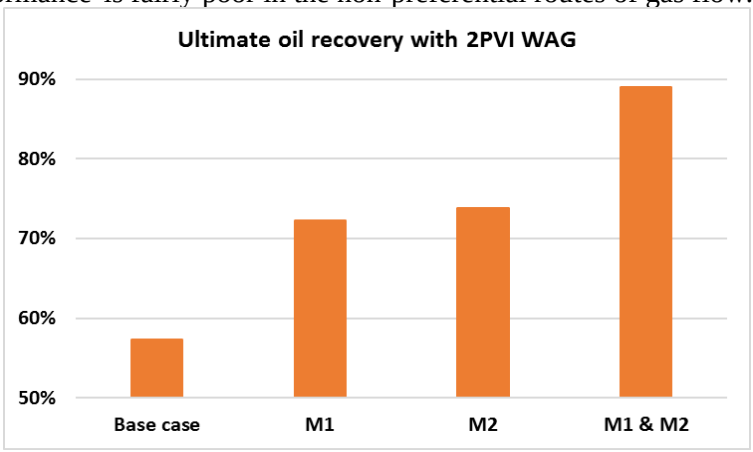

Figure 6 *Ultimte oil recovery.*

On the other hand, IFT effects could work on both preferential routes and non-preferential routes. Unlike oil-stripping effects, IFT effects are not dependent on continuous contact between oil and CO_2.

Instead, the remaining oil is mobilised by IFT effects (increased K_{ro} by layer flow; Sorbie and van Dijke, 2010) and can be efficiently produced by subsequent water injection. Under immiscible conditions (Figure 5C), the oil with lowered viscosity (more CO_2 dissolution) in the preferential routes can be more efficiently produced after the injection 2PV. Under near-miscible conditions (Figure 5D), the combined mechanisms work in tandem to improve the overall displacement performance achieving the highest ultimate oil recovery (Figure 6).

Conclusions

1. Oil stripping effects (M1) can improve the displacement efficiency in the preferential routes only. This is because this mechanism is highly dependent on continuous contact between oil and CO_2.
2. Under immiscible conditions, the oil with lowered viscosity (more CO_2 dissolution) in the preferential routes can be produced by IFT effects.
3. Under near-miscible conditions, we find that the remaining oil in the non-preferential routes may be mobilised by IFT effects and then efficiently produced by the means of WAG injection. As a result, the combined mechanisms work in tandem to significantly improve the displacement performance and therefore the ultimate oil recovery.
4. We point out the importance of both mechanisms M1 and M2 in predicting the oil recovery and the distribution of residual oil in CO_2 WAG process.

Acknowledgements

The authors would like to gratefully acknowledge the funding for this study by the sponsor of the "BICCO2" project at Heriot-Watt University (Petronas and Uzma). Energi Simulation is thanked for funding the chair in Reactive Flow Simulation at Heriot-Watt University held by Eric Mackay. CMG Ltd. is thanked for the use of the GEM simulator.

References

Aziz, K. and Settari, A. (1979) *Petroleum Reservoir Simulation*, Applied Science Publ. Ltd., London, UK.

CMG (2017) 'CMG-GEM technical manual' in *Computer Modelling Group*.

Coats, K. H. (1980) 'An Equation of State Compositional Model', *Society of Petroleum Engineers Journal*.

Dykstra, H. and Parsons, R. (1950) 'The prediction of oil recovery by waterflood', *Secondary recovery of oil in the United States*, 2, 160-174.

Orr, F. M. (2007) *Theory of gas injection processes*, Tie-Line Publications.

Sohrabi, M., Danesh, A., Tehrani, D. H. and Jamiolahmady, M. (2008a) 'Microscopic Mechanisms of Oil Recovery By Near-Miscible Gas Injection', *Transport in Porous Media*, 72(3), 351-367.

Sorbie, K. S. and van Dijke, M. I. (2010) 'The Mechanism of Oil Recovery by Water-Alternating-Gas Injection at Near-Miscible Conditions in Mixed Wet Systems' in *SPE Improved Oil Recovery Symposium*, Society of Petroleum Engineers.

Stalkup, F. I. (1983) *Miscible displacement, SPE Monograph Volume 8, Henry L. Doherty Series*.